Absolute cross sections for the electron-impact single ionization of Mo^{4+} and Mo^{5+} ions

M. E. Bannister and F. W. Meyer
Physics Division, Oak Ridge National Laboratory, Oak Ridge, Tennessee 38731-6372

Y. S. Chung, N. Djurić, and G. H. Dunn*
Joint Institute for Laboratory Astrophysics of the University of Colorado and the National Institute of Standards and Technology, Boulder, Colorado 80309-0440

M. S. Pindzola
Department of Physics, Auburn University, Auburn, Alabama 36849

D. C. Griffin
Department of Physics, Rollins College, Winter Park, Florida 32789
(Received 16 February 1995)

Absolute total cross sections for the electron-impact single ionization of Mo^{4+} and Mo^{5+} ions have been measured using a crossed-beams technique from below the ground-state ionization threshold to 500 eV with typical total uncertainties of 9% near the peak of the cross sections. Molybdenum ion production in the source was facilitated by a mini-oven sublimating MoO_3. The measured cross sections are in good agreement with distorted-wave calculations and are dominated by contributions from excitation autoionization. Nonzero cross sections below the threshold for ionization of $Mo^{5+}(4p^6 4d)$ ground-state ions indicate that metastable ions were present in the beam extracted from an electron-cyclotron-resonance ion source. No evidence of metastable ions was found in the case of the Mo^{4+} measurements. Ionization rate coefficients and fitting parameters are presented for the experimental data.

PACS number(s): 34.80.Kw

I. INTRODUCTION

Accurate cross sections and rate coefficients for electron-impact ionization of ions are essential for modeling and diagnosing both laboratory and astrophysical plasmas. Despite the wealth of data that exist for ionization [1], cross sections are absent for several key ions of interest to fusion researchers, most notably for heavy refractory metals [2]. In particular, cross sections for ionization and excitation of molybdenum ions in low to medium charge states are needed to understand the edge plasma of fusion devices that use molybdenum in plasma-facing components.

In this paper, we report absolute total cross sections for electron-impact single ionization of Mo^{4+} and Mo^{5+} ions with outer shell configurations of $4s^2 4p^6 4d^2$ and $4s^2 4p^6 4d$, respectively. We are aware of published experimental cross sections for Mo^+ [3]. Cross sections have been published [4] for Zr^{3+}, which is isoelectronic with Mo^{5+}. To our knowledge, there are no published measurements for any ion isoelectronic with Mo^{4+}.

The ionization cross sections reported here were measured using the Oak Ridge National Laboratory (ORNL) electron-ion crossed-beams apparatus. In addition, distorted-wave calculations for direct and total ionization are presented and compared to the measurements.

II. EXPERIMENT

The experimental method and ORNL crossed-beam apparatus have been described in detail elsewhere [5,6], so only a brief overview will be presented here. A schematic drawing of the apparatus is shown in Fig. 1.

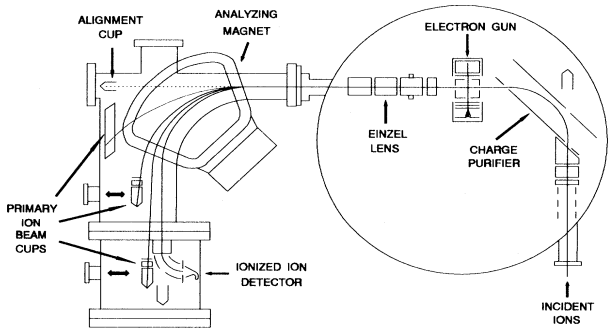

FIG. 1. Electron-ion crossed-beams experimental apparatus. See text for an explanation.

*Quantum Physics Division, National Institute of Standards and Technology.

A recent modification to the electron-cyclotron-resonance (ECR) ion source to enable production of intense, stable beams of metal ions is discussed in some detail.

A. Ion and electron beams

The Mo ion beams used in the present experiment were produced using a mini-oven [7] which is incorporated into the end of the central electrode of the coaxial microwave injection waveguide, located immediately adjacent to the main plasma stage of the ECR source. The oven consists of a hollow boron nitride body with machined grooves into which are wound about ten turns of 0.5 mm diameter Ta wire. The boron nitride source body plus heater coil is surrounded by a cylindrical Mo heat shield 15 mm in diameter and roughly 50 mm in length, which also serves as the termination of the 15 mm diameter coaxial electrode. The maximum temperature attainable with this oven is about 1250 °C, requiring a heater power of about 85 W. While sufficient for direct evaporation of many metallic species, including Pb, Au, Fe, and Ni, it is clearly insufficient for direct evaporation of Mo, which requires temperatures in excess of 2000 °C to reach the 10^{-2} Pa (10^{-4} Torr) vapor pressure range required for production of intense, low-charge-state metallic-ion beams.

As a result, MoO_3, a volatile metal oxide powder, was used instead. MoO_3 has a 10^{-2} Pa (10^{-4} Torr) vapor pressure already at a temperature slightly above 500 °C, which is well within the capability of the mini-oven. The powder was tamped into an open-ended cylindrical Mo crucible (5.7 mm o.d., 3 mm i.d., length 25 mm) around a central rod which is subsequently removed to maximize the exposed powder surface from which vapor is generated. This "hollow charge" technique was found by trial and error and gave good beam intensities as well as quite good charge lifetimes. Subsequent to filling of the crucible, it is inserted into the boron nitride oven body, after a Mo end plug has been inserted in back and a Mo nozzle (about 5 mm long with a 1.2 mm orifice) in front to limit conductance of vapor out of the oven at the operating temperature. With this charge configuration and a heater power level of 22 W, it was found that stable, intense beams of Mo^{4+} and Mo^{5+} could be obtained, with oven charge lifetimes approaching 40 h. Required microwave power levels were very low: approximately 20 W for +4 and +5 charge state production, and 50 W for +14. With He as a support gas and 3×3 mm entrance and exit slits for our analyzing magnet (required to resolve the individual Mo isotopes), total beam currents in the range of 1–5 μA could be obtained for charge states up to +16. Only Mo ions of mass 98 amu, comprising about one-quarter of the natural abundance [8], were used for the present investigation.

Molybdenum ions are extracted from the ion source at 10 kV and mass analyzed by a 90° bending magnet. Components of the ion beam produced by charge exchange reactions along the few-meter beamline between this mass analyzer and the collision volume are eliminated by a parallel-plate analyzer (charge purifier) just before entering the collision volume, where the ion beam is crossed perpendicularly with an electron beam. A double-focusing magnet located downstream of the collision volume separates the product $Mo^{(q+1)+}$ ions from the primary Mo^{q+} ion beam, deflecting the product ions through 90°. The product ions are then electrostatically deflected 90° out of the plane of the magnetic dispersion and onto a channel electron multiplier. The primary molybdenum ions are collected by one of three Faraday cups (two are movable) shown in Fig. 1. The cup used and its position depend on the charge ratio of the primary and product ions. For the Mo^{4+} and Mo^{5+} measurements, the middle Faraday cup was used.

The electron beam is generated as follows. Electrons from an indirectly heated cathode are electrostatically focused into a beam. An immersion lens draws the electrons from the cathode into a focus and a cylinder-aperture (rectangular geometry) lens makes the beam parallel [9]. The gun, collision volume, and collector are magnetically shielded to reduce fields in these regions to less than 40 mG. After passing through the collision volume, the electrons are driven by a transverse electric field onto a collector plate covered with a metal "honeycomb." The electron current to the box surrounding the collision volume is less than 1% of the total collector electron current. For electron energies less than 150 eV, a fraction of the electron current passing through the collision volume strikes a shielding electrode between the collision volume and the collector. Electron-beam profile measurements demonstrate that some of the electrons striking this shield pass through the ion beam. Thus the measured electron current is taken to be the sum of the currents to the collector and the shield. The electron beam is chopped at 100 Hz during data acquisition by applying a square-wave voltage to the extraction electrode of the gun.

The differential distributions (profiles) of the electron and ion beams in the plane perpendicular to both beams are measured using a stepping-motor-driven L-shaped beam probe with coplanar slits, each 0.15 mm wide. Combinations of these current profiles are integrated numerically to obtain the "form factor," the geometric term quantifying the overlap of the two beams [9].

B. Cross sections and uncertainties

The absolute cross sections are determined [10] from the measurements using

$$\sigma(E) = \frac{R}{I_i I_e} \frac{qe^2 v_i v_e}{\sqrt{v_i^2 + v_e^2}} \frac{F}{D}, \tag{1}$$

where $\sigma(E)$ is the absolute cross section at the center-of-mass electron-impact energy E, R is the product ion count rate, I_i and I_e are the incident ion and electron currents, qe is the charge of the incident ions, v_i and v_e are the incident ion and electron velocities, F is the form factor that is determined from the two beam profiles, and D is the detection efficiency for the product ions that we estimated to be 98% [11].

TABLE I. Configuration-average ionization potentials for Mo^{4+} and Mo^{5+}.

Ion	Configuration	Subshell	Ionization potential (eV)
Mo^{4+}	$4s^2 4p^6 4d^2$	$4d$	53.3
		$4p$	94.1
		$4s$	126.3
Mo^{5+}	$4s^2 4p^6 4d$	$4d$	68.5
		$4p$	109.8
		$4s$	142.8

III. RESULTS

Absolute total cross sections for electron-impact single ionization of Mo^{4+} and Mo^{5+} were measured from below the ground-state thresholds to 500 eV. Heating of the electron collector led to pressure loading of the apparatus at higher electron energies and currents and thus prevented extending the measurements beyond 500 eV. Calculations were performed over the same energy range for direct and total ionization using the configuration-average distorted-wave (CADW) method [12]. For these ions, the effects of energy-level splitting within the configurations, interference between the direct and indirect channels, and radiative stabilization of autoionizing states are all assumed to be small. Direct ionization of electrons from the $4d$, $4p$, and $4s$ subshells is included, using the calculated thresholds given in Table I. The transitions to autoionizing configurations included in the calculation of the total ionization cross section are given in Table II, with configuration-average excitation energies and calculated excitation cross sections at threshold. The required bound radial orbitals and energy eigenvalues were obtained using Cowan's Hartree-Fock atomic wave-function code [13].

A. Mo^{4+}

Measured and calculated absolute total cross sections for electron-impact single ionization of Mo^{4+} are shown in Fig. 2. Points represent measurements, the dashed curve represents the CADW calculations for direct ionization from the $4p^6 4d^2$ ground state, and the solid curve represents the theoretical results for all relevant processes (direct ionization plus excitation autoionization). The experimental data are also presented in Table III.

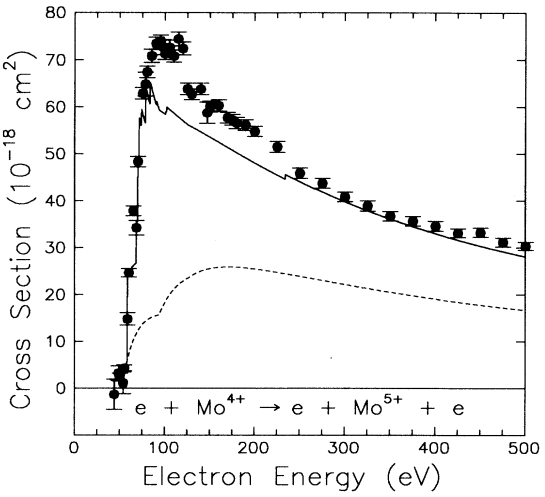

FIG. 2. Absolute cross sections as a function of electron-impact energy for the single ionization of Mo^{4+}. The present experimental results are indicated by the solid circles with relative uncertainties at the one-standard-deviation level. The curves are the results of configuration-average distorted-wave calculations: dashed curve, direct ionization only; solid curve, direct ionization plus excitation autoionization.

The error bars shown in Fig. 2 are relative uncertainties only and are displayed at the one-standard-deviation level. Relative uncertainties are comprised of counting statistical uncertainties in the measurements and a 2% uncertainty from form factor variations. These relative uncertainties are also listed in Table III. In addition to the relative uncertainties, there are a number of systematic uncertainties associated with the absolute value of the form factor (4%), transmission of product ions to the

TABLE II. Excitation cross sections for Mo^{4+} and Mo^{5+} in the ground configuration. These configuration-average distorted-wave calculations were used in the theory curves of Figs. 2 and 3. Only transitions whose average excitation energies lie above the ionization potential are included in the calculations.

	Average excitation energy (eV)		Cross section at threshold (10^{-18} cm^2)	
Transition	Mo^{4+}	Mo^{5+}	Mo^{4+}	Mo^{5+}
$4p \rightarrow 4f$	70.2	75.2	12.3	14.4
$4p \rightarrow 5p$	58.6	–	17.9	–
$4p \rightarrow 5d$	69.0	76.1	8.8	7.3
$4p \rightarrow 5f$	79.0	87.9	5.2	4.6
$4p \rightarrow 6p$	74.3	83.3	3.7	3.1
$4p \rightarrow 6d$	78.8	89.0	2.6	2.0
$4p \rightarrow 6f$	83.7	95.8	2.5	2.0
$4s \rightarrow 4d$	71.8	73.1	9.3	9.2
$4s \rightarrow 4f$	102.4	107.9	1.1	1.4
$4s \rightarrow 5s$	83.6	88.9	2.3	2.3
$3d \rightarrow 4d$	234.4	237.3	1.0	1.2

channeltron (4%), signal ion detection and pulse transmission (5%), measurement of electron and ion currents (2% each), and electron and ion velocities (1% each). These are combined in quadrature with each other and with the relative uncertainties multiplied by a coverage factor of 2. This yields the total uncertainty shown in parentheses in the last column of Table III. This expanded total uncertainty is estimated to be comparable to a 90% confidence level. As seen in the table, the expanded total uncertainty near the peak of the cross section is typically 9%.

TABLE III. Experimentally measured absolute total cross sections for electron-impact single ionization of Mo^{4+}. The relative uncertainties are at the one-standard-deviation level; the expanded total uncertainties (given in parentheses) are at a high confidence level corresponding to 90% confidence for the relative uncertainties.

E (eV)	σ (10^{-18} cm^2)
44.4	−1.32 ± 3.23 (6.47)
49.3	3.23 ± 1.57 (3.14)
50.7	2.37 ± 0.84 (1.69)
54.3	1.13 ± 2.30 (4.60)
55.7	4.33 ± 0.62 (1.29)
59.1	14.78 ± 1.32 (2.90)
60.6	24.63 ± 0.86 (2.66)
65.6	37.85 ± 1.06 (3.76)
68.9	34.23 ± 1.57 (4.21)
70.6	48.33 ± 1.11 (4.54)
75.5	62.87 ± 1.24 (5.72)
78.6	64.86 ± 2.55 (7.37)
80.4	67.46 ± 1.23 (6.06)
85.4	70.83 ± 1.40 (6.45)
90.4	73.46 ± 1.31 (6.57)
95.3	73.90 ± 1.32 (6.61)
98.1	72.70 ± 1.57 (6.74)
100.3	71.31 ± 1.24 (6.35)
105.2	72.61 ± 1.55 (6.71)
110.2	70.80 ± 1.26 (6.33)
115.2	74.41 ± 1.45 (6.76)
120.2	72.39 ± 1.34 (6.51)
125.3	63.83 ± 1.23 (5.78)
130.0	62.67 ± 1.17 (5.65)
140.2	63.81 ± 1.24 (5.79)
147.3	58.74 ± 2.25 (6.59)
150.3	60.06 ± 1.14 (5.43)
160.1	60.32 ± 1.22 (5.52)
170.1	57.73 ± 1.17 (5.28)
175.2	57.28 ± 1.14 (5.22)
180.2	56.58 ± 1.21 (5.24)
190.2	56.16 ± 1.15 (5.15)
200.3	54.81 ± 1.08 (4.98)
225.3	51.48 ± 1.17 (4.82)
250.3	45.91 ± 1.11 (4.37)
275.3	43.73 ± 1.03 (4.14)
300.3	40.84 ± 1.00 (3.90)
325.4	38.92 ± 1.12 (3.90)
350.5	36.75 ± 1.01 (3.62)
375.5	35.66 ± 1.01 (3.55)
400.5	34.61 ± 1.04 (3.52)
425.4	33.14 ± 0.93 (3.29)
450.5	33.26 ± 0.97 (3.35)
475.5	31.14 ± 0.96 (3.20)
500.4	30.36 ± 0.87 (3.04)

The measured cross sections are about 20% higher than the calculations near the peak, but the difference is only about 10% at 225 eV and just a few percent at energies above 250 eV. This comparison indicates that the ratio of indirect (excitation autoionization) to direct contributions is about 3.6 near the peak of the measured cross sections.

Since the measured cross sections below the ground-state ionization threshold [14] of 54.49 eV are zero within experimental uncertainty, we conclude that no measurable amount of metastables was present in the Mo^{4+} ion beam.

B. Mo^{5+}

Figure 3 illustrates the measured and calculated cross sections for Mo^{5+} from 30 eV to 500 eV, and again the experimental results are also presented in Table IV. Uncertainties are accounted for the same as in the discussion above for Mo^{4+}, and the notations and usage in Fig. 3 is the same as that for Fig. 2.

The inner-shell excitations included in the total ionization calculations, listed in Table II, are the same as for the Mo^{4+} case except that the $4p \rightarrow 5p$ transition is not included since it lies below the ground-state ionization threshold for Mo^{5+}. The CADW results are in good overall agreement with the measurements, although the experimental cross sections are approximately 15% larger near the peak. Above 200 eV, the experiment and the-

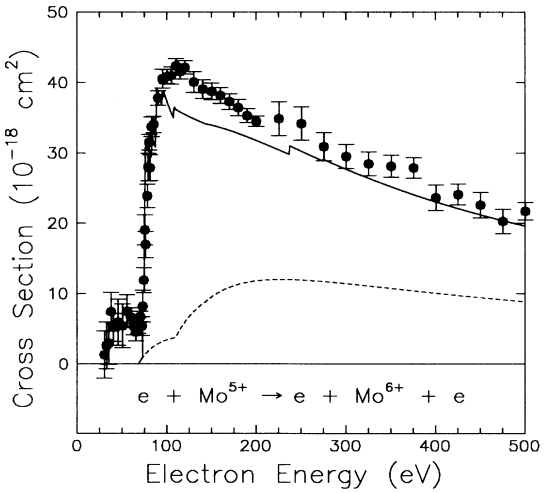

FIG. 3. Absolute cross sections as a function of electron-impact energy for single ionization of Mo^{5+}. The present experimental results are indicated by the solid circles with relative uncertainties at the one-standard-deviation level. The curves are the results of configuration-average distorted-wave calculations: dashed curve, direct ionization only; solid curve, direct ionization plus excitation autoionization.

TABLE IV. Experimentally measured absolute total cross sections for electron-impact single ionization of Mo^{5+}. The relative uncertainties are at the one-standard-deviation level; the expanded total uncertainties (given in parentheses) are at a high confidence level corresponding to 90% confidence for the relative uncertainties.

E (eV)	σ (10^{-18} cm^2)
30.7	1.32 ± 3.34 (6.69)
33.1	2.62 ± 3.33 (6.65)
35.6	2.92 ± 3.00 (6.00)
38.1	7.42 ± 2.75 (5.53)
40.7	5.18 ± 2.00 (4.01)
45.8	5.92 ± 3.26 (6.53)
50.8	5.41 ± 3.11 (6.23)
55.8	7.49 ± 2.32 (4.70)
60.7	6.60 ± 1.38 (2.81)
63.2	5.37 ± 1.26 (2.57)
65.7	4.52 ± 1.24 (2.52)
68.2	5.47 ± 1.12 (2.29)
70.7	6.70 ± 0.74 (1.58)
72.6	5.37 ± 1.33 (2.69)
73.3	8.19 ± 2.25 (4.54)
74.6	11.91 ± 1.78 (3.68)
75.8	19.05 ± 2.14 (4.55)
76.6	16.98 ± 1.85 (3.96)
78.5	23.89 ± 1.67 (3.88)
79.5	28.00 ± 1.96 (4.54)
80.5	31.51 ± 1.09 (3.37)
81.5	27.90 ± 1.83 (4.31)
83.2	33.70 ± 1.40 (3.93)
85.5	34.04 ± 1.16 (3.62)
90.5	37.79 ± 1.05 (3.75)
95.4	40.53 ± 1.34 (4.27)
100.4	40.84 ± 1.00 (3.90)
105.3	40.98 ± 1.23 (4.15)
110.4	42.38 ± 1.02 (4.03)
115.3	41.55 ± 1.07 (4.02)
120.4	42.14 ± 0.95 (3.94)
130.5	40.07 ± 1.49 (4.43)
140.4	39.06 ± 1.32 (4.15)
150.3	38.74 ± 1.20 (3.98)
160.2	38.15 ± 1.16 (3.90)
170.2	37.29 ± 1.13 (3.80)
180.0	36.44 ± 1.16 (3.78)
190.0	35.29 ± 0.98 (3.49)
200.2	34.49 ± 0.76 (3.20)
225.4	34.86 ± 2.41 (5.61)
250.4	34.17 ± 2.37 (5.51)
275.4	30.91 ± 2.01 (4.75)
300.4	29.52 ± 1.71 (4.19)
325.4	28.47 ± 1.68 (4.09)
350.5	28.13 ± 1.56 (3.88)
375.6	27.90 ± 1.45 (3.69)
400.5	23.65 ± 1.81 (4.10)
425.5	24.10 ± 1.48 (3.55)
450.5	22.60 ± 1.81 (4.07)
475.5	20.28 ± 1.74 (3.85)
500.5	21.72 ± 1.24 (3.06)

ory differ by only a few percent, and agree well within the total uncertainty of the measurements.

For this ion the comparison of theory and experiment indicates that near the peak of the measured cross sections, the ratio of indirect (excitation autoionization) to direct contributions is about 10.2, nearly identical to the ratio of 10.5 estimated [4] for the Zr^{3+} measurements. Not surprisingly, the shapes of the cross section curves are also very similar for Mo^{5+} and Zr^{3+}. Comparing the indirect-to-direct ratios for the Mo^{4+} and Mo^{5+} measurements, we note that the relative contribution of excitation autoionization increases as the number of electrons in the outer subshell is reduced from two to one, as was shown [6] for the case of $Kr^{4+}(4s^24p^2)$ and $Kr^{5+}(4s^24p)$.

Nonzero cross sections between 30 eV and the ground-state ionization threshold [14] of 68.83 eV indicate a population of metastable Mo^{5+} ions in the incident beam. Since the ionization potential for the $4p^65s$ configuration is 54.0 eV [14], another metastable configuration must also contribute to the measured cross sections, most likely the $4p^54d^2$ configuration. Because less than one-half of the states in this latter configuration are quartets, and because the relative populations of the two metastable configurations are unknown, a configuration-average calculation for ionization of these metastable ions was not appropriate. However, we estimated the metastable fraction of the Mo^{5+} beam using a least-squares fit to $\sigma_j(E) = (A_j/EI_j)\ln(E/I_j)$ for the ground and metastable cross sections, where A_j is a constant, I_j is the ionization potential, and the subscript j denotes either the ground or metastable configurations. This functional form is the same as the Lotz [15] formulation, except that the constant term A_j is determined by a fit and not set equal to $4.5 \times 10^{-14}q$ cm^2 eV^2, where q is the number of electrons in the outer subshell. Hence, the "overall" enhancement of ionization cross section by excitation autoionization can be included. The least-squares fit produced values of $(1.43 \pm 1.69) \times 10^{-14}$ cm^2 eV^2 and $(46.1 \pm 0.3) \times 10^{-14}$ cm^2 eV^2 for A_m and A_g, respectively, with a fitted metastable threshold I_m of 29.4 eV. These numbers yield a metastable fraction of 0.030 ± 0.035 for the Mo^{5+} ion beam. In contrast, using the unmodified Lotz [15] formula coefficient for the metastable cross section (assuming direct ionization of two $4d$ subshell electrons with an ionization potential of 29.4 eV) and comparing the prediction with the measured value just below the ground state ionization threshold, one would estimate the metastable fraction to be about 0.15. This is probably an overestimate, since the Lotz formula is known to significantly underestimate the total ionization cross section of multicharged ions, particularly when excitation autoionization is important.

Without an appropriate calculation for indirect ionization of the metastable ions and due to the large uncertainty in the metastable fraction, we feel that subtraction from the measured data of a fitted curve representing the metastable contribution would be inappropriate. However, we do note that the contribution from the metastable ions may account for much of the difference between the measured cross sections and those calculated for ground configuration ions.

TABLE V. Maxwellian rate coefficients (in units of cm^3/s) for the ionization of Mo^{4+} and Mo^{5+} at selected values of T (in K) calculated from the measured cross sections (see text).

Electron temperature T (K)	Ionization rate coefficients α (cm^3/s) Mo^{4+}	Mo^{5+}
1.0×10^4	1.62×10^{-31}	2.14×10^{-24}
2.0×10^4	2.68×10^{-20}	8.33×10^{-17}
4.0×10^4	1.21×10^{-14}	5.63×10^{-13}
6.0×10^4	1.35×10^{-12}	1.10×10^{-11}
8.0×10^4	1.71×10^{-11}	4.92×10^{-11}
1.0×10^5	8.34×10^{-11}	1.25×10^{-10}
2.0×10^5	2.23×10^{-9}	1.24×10^{-9}
4.0×10^5	1.16×10^{-8}	6.12×10^{-9}
6.0×10^5	1.96×10^{-8}	1.10×10^{-8}
8.0×10^5	2.51×10^{-8}	1.47×10^{-8}
1.0×10^6	2.88×10^{-8}	1.74×10^{-8}
2.0×10^6	3.59×10^{-8}	2.38×10^{-8}
4.0×10^6	3.63×10^{-8}	2.66×10^{-8}
6.0×10^6	3.44×10^{-8}	2.71×10^{-8}
8.0×10^6	3.24×10^{-8}	2.70×10^{-8}
1.0×10^7	3.08×10^{-8}	2.67×10^{-8}
2.0×10^7	2.51×10^{-8}	2.49×10^{-8}
4.0×10^7	1.97×10^{-8}	2.22×10^{-8}
6.0×10^7	1.69×10^{-8}	2.04×10^{-8}
8.0×10^7	1.52×10^{-8}	1.91×10^{-8}
1.0×10^8	1.39×10^{-8}	1.80×10^{-8}

IV. RATE COEFFICIENTS

For many applications such as plasma modeling, it is useful to report Maxwellian rate coefficients for the process investigated. Table V lists rate coefficients calculated from our present cross section measurements using a method described elsewhere [16]. In addition, the rate coefficients were fit with Chebyshev polynomials of the first kind $T_n(x)$ to enable the user to calculate them for any temperature in the range 10^4 K $\leq T \leq 10^8$ K:

$$\alpha(T) = T^{1/2} e^{-I/kT} \sum_{j=0}^{n} a_j T_j(x) \qquad (2)$$

where I is the ionization potential. The coefficients $a_0, \ldots, a_{10}$ given in Table VI reproduce the rate coefficients to within 2% over the temperature range 4×10^4 K $\leq T \leq 10^8$ K. The rate coefficient $\alpha(T)$ can be expressed simply as

$$\alpha(T) = \tfrac{1}{2} T^{1/2} e^{-I/kT} (b_0 - b_2) \qquad (3)$$

with the coefficients b_0 and b_2 calculated using Clenshaw's algorithm [17]

$$b_j = 2x b_{j+1} - b_{j+2} + a_j, \quad j = 0, 1, 2, \ldots, 10 \qquad (4)$$

TABLE VI. Rate-coefficient fitting parameters. All parameters are in units of 10^{-13} cm^3 $K^{-1/2}$ s^{-1}. Rate coefficients in the range 10^4 K $\leq T \leq 10^8$ K may be calculated using these parameters in a Chebyshev polynomial expansion, or through Clenshaw's algorithm (see text).

Fitting parameter	Mo^{4+}	Mo^{5+}
a_0	524.768	287.613
a_1	−197.815	−108.332
a_2	−145.226	−25.2187
a_3	62.6551	−23.5501
a_4	101.424	44.1255
a_5	−85.1852	−0.335764
a_6	−9.49660	−20.5757
a_7	47.5461	3.19604
a_8	−23.9673	9.78014
a_9	−10.7326	−1.62661
a_{10}	12.4024	−3.16169

where $b_{11} = b_{12} = 0$ and the reduced energy x is given by

$$x = \frac{\log_{10} T - 6}{2} \quad . \qquad (5)$$

V. SUMMARY

Absolute total cross sections for electron-impact single ionization of Mo^{4+} and Mo^{5+} ions were measured using the ORNL crossed-beams apparatus, with typical total uncertainties of 9%. The cross sections were also calculated using the CADW method with both direct and indirect processes included. Measured and calculated values are in good agreement, and excitation autoionization is found to enhance the cross section by factors of 3.6 (Mo^{4+}) and 10.5 (Mo^{5+}) near the cross section peaks. A metastable fraction of a few percent was indicated for the Mo^{5+} ion beam; an absence of metastables was inferred for the Mo^{4+} ion beam.

ACKNOWLEDGMENTS

The authors wish to thank C. C. Havener for valuable discussions and J. W. Hale for skilled technical assistance. This work was supported by the Division of Applied Plasma Physics, Office of Fusion Energy of the U.S. Department of Energy under Contract No. DE-AC05-84OR21400 with Martin Marietta Energy Systems, Inc., and Contract No. DE-A105-86ER532237 with the National Institute of Standards and Technology. M.E.B. acknowledges ORNL and the Oak Ridge Institute for Science and Education for financial support.

[1] R. K. Janev, M. F. A. Harrison, and H. W. Drawin, Nucl. Fusion **29**, 109 (1989).
[2] R. A. Phaneuf, Phys. Scripta T **47**, 124 (1993).
[3] K. F. Man, A. C. H. Smith, and M. F. A. Harrison, J. Phys. B **20**, 1351 (1987).
[4] R. A. Falk, G. H. Dunn, D. C. Gregory, and D. H. Crandall, Phys. Rev. A **27**, 762 (1983).
[5] D. C. Gregory, F. W. Meyer, A. Müller, and P. Defrance,

Phys. Rev. A **34**, 3657 (1986).
[6] M. E. Bannister, X. Q. Guo, and T. M. Kojima, Phys. Rev. A **49**, 4676 (1994).
[7] D. Hitz, G. Melin, M. Pontonnier, and T. K. Nguyen, KVI Report No. 996, 1993 (unpublished).
[8] *Handbook of Chemistry and Physics*, 67th ed., edited by R. C. Weast, M. J. Astle, and W. H. Beyer (CRC Press, Boca Raton, FL, 1986).
[9] G. H. Dunn and B. Van Zyl, Phys. Rev. **154**, 40 (1967).
[10] See, for example, M. F. A. Harrison, J. Appl. Phys. **17**, 371 (1966).
[11] D. C. Gregory, P. F. Dittner, and D. H. Crandall, Phys. Rev. A **27**, 724 (1983).
[12] M. S. Pindzola, D. C. Griffin, and C. Bottcher, in *Physics of Electron-Ion and Ion-Ion Collisions*, Vol. 145 of NATO *Advanced Study Institute, Series B: Physics*, edited by F. Brouillard (Plenum, New York, 1986), p. 75.
[13] R. D. Cowan, *The Theory of Atomic Structure and Spectra* (California Press, Berkeley, 1981).
[14] J. Sugar and A. Musgrove, J. Phys. Chem. Ref. Data **17**, 155 (1988).
[15] W. Lotz, Z. Phys. **206**, 205 (1967).
[16] D. H. Crandall, G. H. Dunn, A. Gallagher, D. G. Hummer, C. V. Kunasz, D. Leep, and P. O. Taylor, Astrophys. J. **191**, 789 (1974).
[17] C. W. Clenshaw, Math. Tables Comput. **9**, 118 (1955).